Journal of Materials Chemistry

www.rsc.org/materials

Volume 20 | Number 31 | 21 August 2010 | Pages 6369–6572

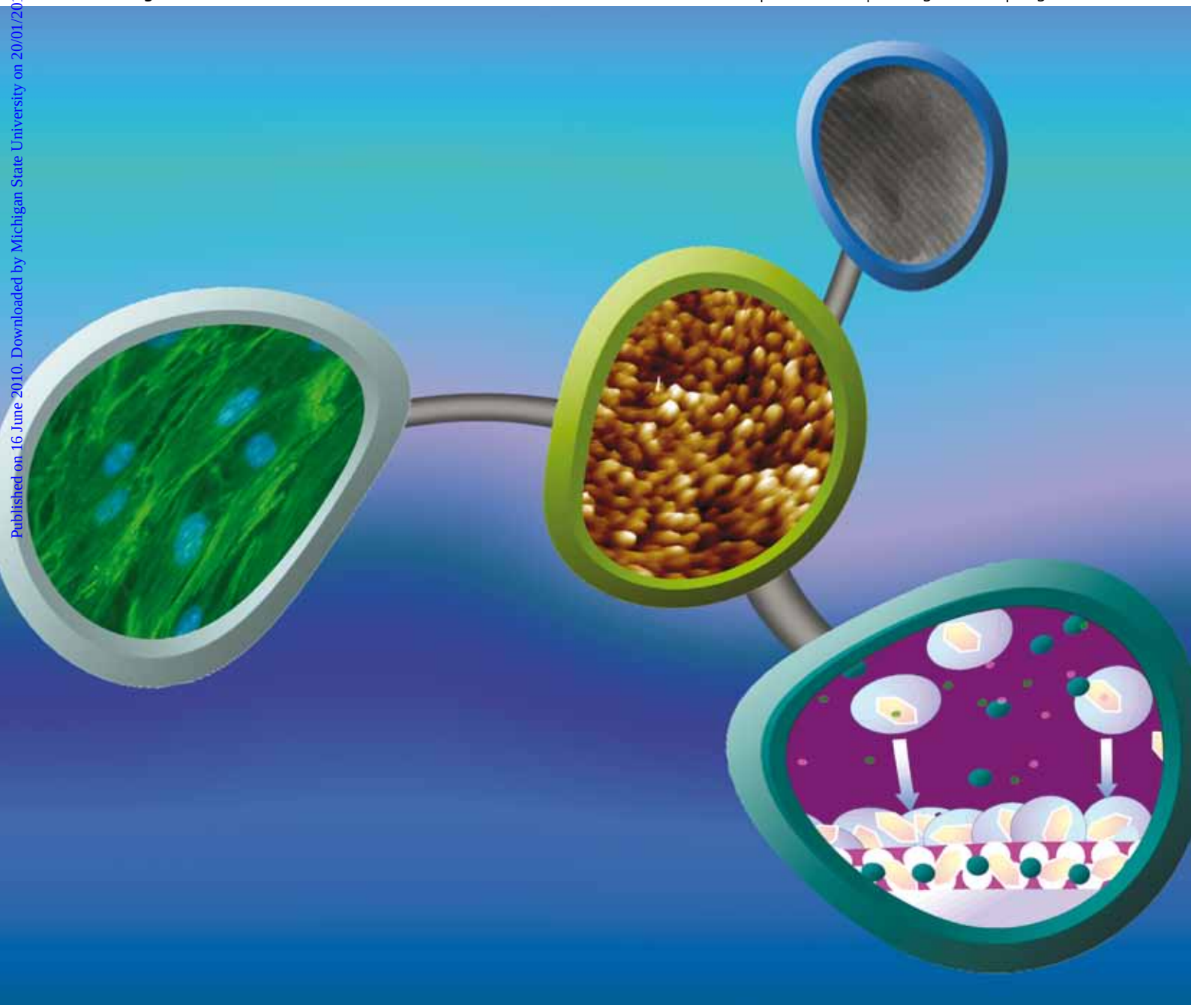

ISSN 0959-9428

RSC Publishing

0959-9428(2010)20:31;1-N

Mesoporous bioactive glass coatings on stainless steel for enhanced cell activity, cytoskeletal organization and AsMg immobilization†

Xiupeng Wang,*[a] Xia Li,[a] Kazuo Onuma,[a] Atsuo Ito,[a] Yu Sogo,[a] Katsunori Kosuge[b] and Ayako Oyane[c]

Received 12th February 2010, Accepted 28th April 2010
DOI: 10.1039/c0jm00399a

Mesoporous bioactive glass (MBG) coatings with SiO_2 : CaO : P_2O_5 mol ratio of 100 : 0 : 0, 80 : 15 : 5 and 70 : 25 : 5 and a tunable pore size and pore structure were prepared on a stainless steel plate by spin-coating sol solutions containing a triblock copolymer and the inorganic precursors. The calcium content in the MBG coatings affected the mesoporous structure. With the increase in calcium content, the crystallinity of the MBG coatings increased and thus the Brunauer–Emmett–Teller (BET) surface area and pore volume decreased. The MBG coatings were evaluated on the basis of protein adsorption, cell attachment, cell proliferation, cell differentiation, cytoskeletal organization and L-ascorbic acid phosphate magnesium salt *n*-hydrate (AsMg) immobilization for their potential in improving implant-bone integration. The results showed that the osteoblast MC3T3-E1 cells were stimulated by the mesoporous structure and chemical composition of the MBG coatings, with enhanced cell attachment, proliferation, differentiation and better developed cytoskeleton. Moreover, AsMg was successfully immobilized on the MBG coatings by using an AsMg-containing supersaturated calcium phosphate solution. The AsMg immobilized on the MBG coatings was not denatured and showed high activity enhancing the fibroblast NIH3T3 proliferation *in vitro*. An appropriate range of pore size and a preferred alignment of the mesochannels of the MBG coatings on stainless steel are promising to improve the implant-bone integration.

Introduction

Metals and alloys are widely used in orthopaedic and dental fields as components of artificial implants or restored materials. Metal- and alloy-based orthopaedic implants are generally characterized by their excellent biocompatibility and mechanical properties. However, metals and alloys have some serious shortcomings, for example, a limited corrosion resistance in human body and a lack of bioactivity.[1] A bioactive coating on metals and alloys would be an ideal route to combine good mechanical properties, corrosion resistance, biocompatibility, bioactivity with osseointegration property in one material.[1,2] Moreover, *in vitro* cell responses provide a valuable indication of the *in vivo* behaviour of an implant surface,[3,4] since the actual biological interaction *in vivo* is a cell-mediated event. Cell responses, such as proliferation, differentiation, apoptosis and cytoskeletal organization mainly depend on the texture (both in bulk and surface) and chemical composition of an implant.[5–12] For instance, the bulk texture and chemical composition of the implant affected the ion release, protein adsorption and the cell attachment, gene expression, proliferation and differentiation.[7–12] On the other hand, nanosized surface texture, such as islands, grooves and pits in the individual size range of 5–500 nm, have been reported to affect cells in a variety of ways and change cell attachment, morphology, gene expression, proliferation, differentiation and cytoskeletal organization[13–17] because of the similarity in nanosized features between the implant surface and the natural extracellular matrix (*e.g.*, nano-stripes in collagen).[13–17]

The mesoporous bioactive CaO–P_2O_5–SiO_2 glass (MBG) coating was a good candidate to combine the nanosized texture (both in bulk and surface) with chemical composition. Herein, we prepared MBG coatings with a tunable pore size and pore texture (three-dimensional (3D) pore texture and two-dimensional (2D) pore texture) and with SiO_2 : CaO : P_2O_5 mol ratio of 100 : 0 : 0, 80 : 15 : 5 and 70 : 25 : 5 on stainless steel and evaluated on the basis of protein adsorption, cell attachment, cell proliferation, cell differentiation, cytoskeletal organization and L-ascorbic acid phosphate magnesium salt n-hydrate (AsMg) immobilization.

2. Experimental

2.1 Preparation of stainless steel plates

Commercially available 316 stainless steel sheets (1 × 100 × 300 mm, Nilaco Corporation, Japan) were cut into square plates (1 × 11 × 11 mm) using a silicon carbide blade. The stainless steel plates were washed with acetone for 30 min in an ultrasonic cleaner and then dried at room temperature.

2.2 Preparation of mesoporous bioactive glass (MBG) coatings

The MBG coatings were prepared on the stainless steel plates using an amphiphilic triblock copolymer poly(ethylene

[a]*Institute for Human Science and Biomedical Engineering, National Institute of Advanced Industrial Science and Technology (AIST), Central 6, 1-1-1 Higashi, Tsukuba, Ibaraki, 305-8566, Japan. E-mail: xiupengw@hotmail.com; xp-wang@aist.go.jp; Fax: +81-29-861-6149; Tel: +81-29-861-6072*
[b]*Research Institute for Environmental Management, National Institute of Advanced Industrial Science and Technology (AIST), 16-1 Onogawa, Tsukuba, Ibaraki, 305-8569, Japan*
[c]*Nanotechnology Research Institute, National Institute of Advanced Industrial Science and Technology (AIST), Central 4, 1-1-1 Higashi, Tsukuba, Ibaraki, 305-8562, Japan*
† Electronic supplementary information (ESI) available: Tables S1 and S2 and Fig. S1–S4. See DOI: 10.1039/c0jm00399a

oxide)-poly(propylene oxide)-poly(ethylene oxide) ($EO_{106}PO_{70}EO_{106}$; F127, Anaspec) or $EO_{20}PO_{70}EO_{20}$ (P123, Aldrich) as the templates by evaporation-induced self-assembly (EISA). Tetraethyl orthosilicate (TEOS), calcium chloride, triethyl phosphate (TEP), ethanol, 1 M HCl and one of the above-listed triblock polymers were mixed at a molar ratio of ($CaO + P_2O_5 + SiO_2$) : ethanol : HCl : triblock polymer = 1 : 20 : 0.001 : 0.009 and stirred at room temperature for 2 h to obtain the coating solution. The coating solution (30 μL/plate) was deposited on the stainless steel plate by spin-coating at 1000 rpm for an initial 10 s and then at 3000 rpm for 10 s. The stainless steel plate with the coating was left at room temperature for 12 h to evaporate the volatile components in the coating. Then, the coatings were heated from room temperature to 300 °C at a heating rate of 0.5 °C h^{-1}, and annealed at 300 °C for 3 h. This procedure removed the residual water and organic moieties from the coating. All the specimens were sterilized at 160 °C for 3 h in a drying sterilizer (Model SG600, Yamato Scientific, Co., Ltd.). The coatings with $SiO_2 : CaO : P_2O_5$ mol ratio of 100 : 0 : 0, 80 : 15 : 5 and 70 : 25 : 5 prepared in the presence of F127 were designated as F0, F20 and F30, respectively. The coating with $SiO_2 : CaO : P_2O_5$ mol ratio of 80 : 15 : 5 prepared in the presence of P123 was designated as P20. The coatings with $SiO_2 : CaO : P_2O_5$ mol ratio of 100 : 0 : 0, 80 : 15 : 5 and 70 : 25 : 5 prepared without F127 or P123 were designated as N0, N20 and N30, respectively.

2.3 Characterization of the MBG coatings

The surfaces of the MBG coatings were observed by atomic force microscopy (AFM, Nanoscope III-a, Digital Instruments, USA). The phase composition of the MBG coating was analyzed by thin-film X-ray diffraction (TF-XRD) employing a Cu-Kα X-ray source at 40 kV and 300 mA using a thin-film X-ray diffractometer (Model RINT 2400; Rigaku, Japan). Low-angle X-ray diffraction patterns were obtained at 40 kV and 100 mA. Nanotextures in the MBG coatings were observed by transmission electron microscopy (TEM, TOPCON EM-002B and Hitachi H-9000NA, Japan). For the TEM observation, MBG coatings were detached from the stainless steel plate and dispersed in ethanol, then deposited and dried on a carbon-coated copper grid. N_2 adsorption/desorption isotherms were obtained at −196 °C on an automatic surface area analyzer (BELSORP 28, BEL, Japan) under continuous adsorption conditions. Prior to the N_2 adsorption/desorption study, MBG coatings detached from the stainless steel plates were heated to 160 °C and then outgassed to 10^{-3} Torr at room temperature. Brunauer–Emmett–Teller (BET) analysis was used to determine the total specific surface area (S_{BET}). The total pore volume (V_{total}) was calculated by a t-plot analysis. The Barrett–Joyner–Halenda (BJH) method was used to calculate mesopore size distribution.

2.4 Protein adsorption on MBG coatings

The amount of proteins adsorbed on MBG-coated stainless steel plates was determined by immersing each specimen in 2.0 mL of α-modified minimum essential medium supplemented with 10% fetal bovine serum (αMEM + 10% FBS) in a well of a 24-well culture plate in a humidified atmosphere of 5% CO_2 at 37 °C for 2 h. After the 2 h incubation, each MBG-coated stainless steel plate was gently rinsed with phosphate-buffered saline (PBS(-)) at room temperature. Adsorbed proteins were desorbed by dissolving the MBG coating in 3 mL of 10 mM citric acid solution for 2 h. The desorbed protein was quantified by the Bradford method using a Bio-Rad protein assay dye reagent concentrate (Bio-Rad Laboratories, Inc., Japan) in accordance with the manufacturer's instructions.

2.5 *In vitro* evaluation of the MBG coatings using osteoblastic MC3T3-E1 cells

2.5.1 Osteoblastic MC3T3-E1 cell attachment to the MBG coatings. The attachment of osteoblastic MC3T3-E1 cells (Riken BioResource Center, Japan) to the surface of the MBG coatings was evaluated. 1 mL of osteoblastic MC3T3-E1 cell suspension (1.5×10^5 cells mL^{-1}) were seeded onto the 24-well cell culture plates in which the MBG-coated stainless steel plates were placed and incubated in a humidified atmosphere of 5% CO_2 at 37 °C for 1 and 2 h. The MBG-coated stainless steel plates were removed and rinsed in the culture medium to eliminate the unattached cells. The number of cells attached on the MBG coatings was determined by the WST-8 method using a CCK-8 kit (Dojindo Laboratories, Japan) in accordance with the manufacturer's instructions. Notably, the well size of the 24-well cell culture plates were larger than the MBG-coated stainless steel plates, so some cells attached to the 24-well cell culture plates.

2.5.2 Osteoblastic MC3T3-E1 cell cultures. First, 100 μL of osteoblastic MC3T3-E1 cell suspension (10^5 cells mL^{-1}) was placed on the MBG-coated stainless steel plates and allowed to stand in a humidified atmosphere of 5% CO_2 at 37 °C for 2 h for cell attachment. In this case, most of the cells attached to the MBG-coated stainless steel plates after 2 h. Then, 900 μL of medium (α-MEM + 15% FBS, containing 10 mM sodium β-glycerophosphate, 10 nM dexamethasone and 82 μg mL^{-1} vitamin C) was added to the wells. The cells were cultured in a humidified atmosphere of 5% CO_2 at 37 °C for 3 days. The cell culture medium was quantitatively analyzed for calcium, silicate and phosphorus using an inductively coupled plasma atomic emission spectrometer (ICP: SPS7800, Seiko Instruments, Inc., Japan).

2.5.3 Osteoblastic MC3T3-E1 cell proliferation and differentiation on the MBG coatings. The osteoblastic MC3T3-E1 cells were cultured by the same method described in section 2.5.2, except that the culture time was prolonged to 7 days, with the spend medium replaced every 3 days. After washing twice with PBS(-), the proliferation level of the osteoblastic MC3T3-E1 cells was determined by the WST-8 method using a CCK-8 kit (Dojindo Laboratories, Japan) in accordance with the manufacturer's instructions. The differentiation level of the osteoblastic MC3T3-E1 cells after 7 days of culture was determined on the basis of alkaline phosphatase (ALP) activity, an early marker of osteoblastic cell differentiation and a measure of the bone-forming ability of osteoblast cells. An aliquot of 300 μL of 0.05% Triton X was added to the culture well and the mixture was incubated at 4 °C for 2 h. Then, the supernatant was assayed for ALP activity using a LaboassayTM ALP kit (Wako Pure

Chemicals, Japan) in accordance with the manufacturer's instructions.

2.5.4 F-actin cytoskeleton development of osteoblastic MC3T3-E1 cells on the MBG coatings. F-actin, a protein relevant to cytoskeletal organization, has been visualized for test specimens by fluorescent staining and fluorescence microscopy (BX51, Olympus, Japan). Briefly, specimens for cytoskeletal staining were prepared as follows. The osteoblastic MC3T3-E1 cells were cultured by the same method described in section 2.5.3. After 7 days of culture, the cells were washed twice with PBS(-), fixed in 2% paraformaldehyde for 20 min, and then washed 3 more times to remove excess paraformaldehyde. Fixed cells were first permeablized with 0.1% Triton-X100 at room temperature for 15 min and washed three times with PBS(-) to reduce nonspecific background. Then, the cells for fluorescent staining were blocked with 1% bovine serum albumin (BSA) at room temperature for 20 min and washed three times with PBS(-). The cytoskeletal component, F-actin, was stained with 120 μL/specimen of fluorescein isothiocyanate (FITC, 1.2 μg mL^{-1}, Sigma, Germany). Lastly, specimens were mounted using DAPI (4′,6-diamidino-2-phenylindole) nuclear stain and stored at 4 °C before imaging.

2.6 Immobilization of AsMg on the MBG coatings

AsMg, which is effective in accelerating tissue repair,[18] was introduced in this study. As a non-acidic form of ascorbate, L-ascorbic acid phosphate magnesium salt *n*-hydrate (AsMg) is converted immediately into ascorbic acid in the presence of phosphatase. AsMg is more stable under oxidative conditions than ascorbic acid salts. Ascorbic acid promotes healthy cell development and contributes to many healing processes associated with infection, disease, injury or surgery. It also helps in the repair and maintenance of healthy cartilage, bones, teeth and gums.[18,19] One stainless steel plate with MBG coating was immersed in 2 mL of supersaturated calcium phosphate solution with a calcium concentration of 3.83 mM at a Ca/P molar ratio of 1.5, a $NaHCO_3$ concentration of 15 mM and AsMg concentration of 20 μg mL^{-1} (Table S1, ESI†) at 37 °C for 24 h to obtain the AsMg-MBG coatings. After the immersion, the AsMg-MBG coatings were gently washed twice by immersion in 2 mL of ultrapure water for 3 min. The AsMg-MBG coatings prepared using the F0, N0, F20, P20, N20, F30 and N30 MBG coatings were designated as AF0, AN0, AF20, AP20, AN20, AF30 and AN30, respectively.

Supersaturated calcium phosphate solution was prepared by mixing ×2.0 Ringer's-AsMg, ×2.0 Solita and Meylon at the mixing ratio of 8.54 : 1.28 : 0.18. The chemical composition of the supersaturated calcium phosphate solution is shown in Table S1 (ESI†). A calcium-containing solution (4.5 mM Ca^{2+}, ×2.0 Ringer's) was obtained by mixing Ringer's solution (Otsuka, 2.25 mM Ca^{2+}) and Conclyte®-Ca (Otsuka, 500 mM Ca^{2+}). ×2.0 Ringer's-AsMg solution was prepared by dissolving AsMg (Wako Pure Chemical Industry Ltd, Japan) in ×2.0 Ringer's followed by filter sterilization using a membrane with a pore size of 0.22 μm (×2.0 Ringer's-AsMg). A phosphate-containing solution (20 mM PO_4^{3-}, ×2.0 Solita) was obtained by mixing Solita®-T No. 2 (Ajinomoto Pharma Co., Ltd., Japan, 10 mM PO_4^{3-}) and Conclyte® solution-PK (Otsuka, 500 mM PO_4^{3-}). An alkalinizer, Meylon®, (Otsuka, 833 mM $NaHCO_3$) was used as received without changing its original concentration. All the solutions used to immobilize AsMg were infusion fluids and injections clinically available in Japan. The advantage of using clinically available infusion fluids and injections as raw materials is that the raw materials are sterile and endotoxin free, and have a low regulational barrier for clinical application.

2.7 Characterization of the AsMg-MBG coatings

2.7.1 Measurements of amounts of AsMg, calcium and phosphorus loaded on the AsMg-MBG coatings. Two stainless steel plates with AsMg-MBG coatings in each group were immersed in 3 mL of a 0.025 mM citric acid at 25 °C for 3 h to extract the AsMg completely by dissolving the composite layer. The complete dissolution of the composite layer was confirmed by scanning electron microscopy (SEM; XL30, FEI Company Japan Ltd., Japan). The amount of AsMg in the citric acid buffer was measured by the UV absorption band intensity of AsMg at 260 nm using a UV–visible spectrophotometer (V-550, Jasco, Japan).

After removing the stainless steel plate with MBG coating, the supersaturated calcium phosphate solutions were supplemented with 50 μL of 1 M hydrochloric acid to dissolve any calcium phosphates precipitate dispersed in the supersaturated calcium phosphate solutions. The calcium and phosphorus ion concentrations were measured using an inductively coupled plasma atomic emission spectrometer (ICP: SPS7800, Seiko Instruments, Inc.). From these concentration data, the amounts of calcium and phosphorus loaded on the MBG coatings were calculated.

2.7.2 Surface characterization of the AsMg-MBG coatings. The surface morphology of the AsMg-MBG coatings was analyzed by SEM at an accelerating voltage of 10 kV after being coated with gold. The phase composition of the AsMg-MBG coatings was analyzed by thin-film X-ray diffractometry (TF-XRD) employing a Cu-Kα X-ray source at 40 kV and 300 mA using a thin-film X-ray diffractometer (Model RINT 2400; Rigaku, Japan).

2.7.3 *In vitro* evaluation of the MBG and AsMg-MBG coatings using fibroblastic NIH3T3 cells. First, 100 μL of fibroblastic NIH3T3 cell suspension (10^5 cells mL^{-1}) was placed on the MBG-coated and AsMg-MBG-coated stainless steel plates and allowed to stand in a humidified atmosphere of 5% CO_2 at 37 °C for 2 h for cell attachment. Then, 900 μL of serum-free Dulbecco's modified essential medium supplemented with L-glutamine (0.3 mg mL^{-1}), bovine serum albumin (1.0 mg mL^{-1}), insulin (10.0 μg mL^{-1}), and transferrin (2.0 μg mL^{-1}) was added to the walls. After culturing in a humidified atmosphere of 5% CO_2 at 37 °C for another 72 h, the density of NIH3T3 cells was determined by the WST-8 method using the CCK-8 kit (Dojindo Molecular Technologies, Japan) in accordance with the manufacturer's instructions. The F-actin of fibroblastic NIH3T3 cells were stained and observed by the same method described in section 2.5.4, except that the cell culture time for fibroblastic NIH3T3 cells was 72 h.

2.8 Statistical analysis

All statistical comparisons were conducted using a 95% confidence interval ($p < 0.05$). Groups of different compositions and groups of different pore textures were conducted using single-factor analysis of variance (ANOVA), respectively. When significant differences were found, Tukey's *post hoc* multiple-comparison test was used to determine the significance of the differences between the mean values of the groups.

3. Results and discussion

MBG coatings with different pore textures and chemical compositions were prepared by the evaporation-induced self-assembly (EISA) process (Fig. 1–4). The MBG coatings can be arranged in different mesoporous textures (3D and 2D) depending on the different triblock copolymers used (F127 or P123).[2,20] F127 favoured the formation of pores connected in a 3D mesoporous texture (Fig. 1–3).[20] F0 showed type IV adsorption isotherm behaviour with a large type H2 hysteresis loop and a pore size of 6.8 nm (Fig. 2 and 3). F20 showed a type IV isotherm with a type H1 hysteresis loop and an increased pore size of 7.9 nm. F30 exhibited a wide pore size distribution of about 2–10 nm. The transmission electron microscopy (TEM) image of F20 showed a 3D mesoporous texture with a pore size of about 8 nm (Fig. 2 and 3). In the 200-nm area atomic force microscopy (AFM) images, the surfaces of the F0 and F20

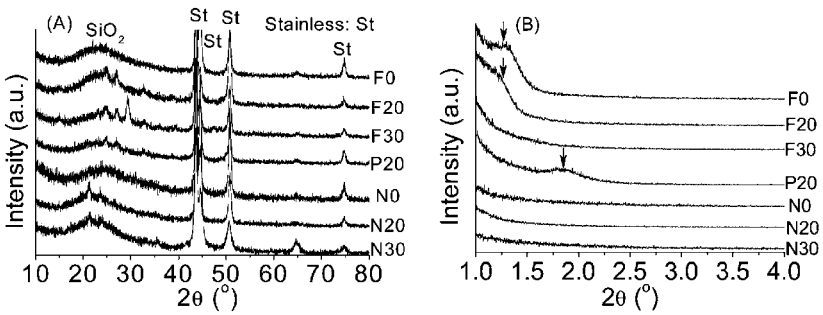

Fig. 1 XRD patterns (A) and low-angle XRD patterns (B) of the MBG coatings.

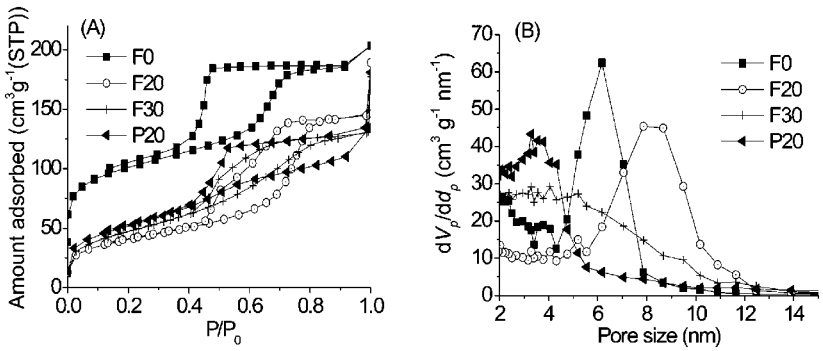

Fig. 2 N_2 adsorption/desorption isotherms (A) and pore size distribution (B) of the MBG coatings.

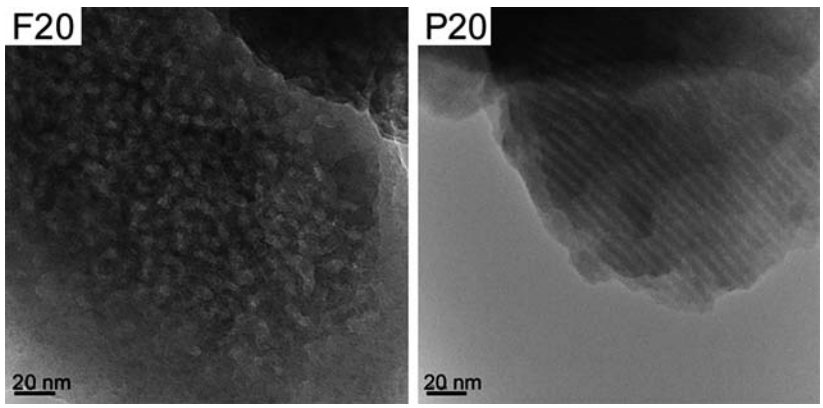

Fig. 3 TEM images of the MBG coatings (F20, P20).

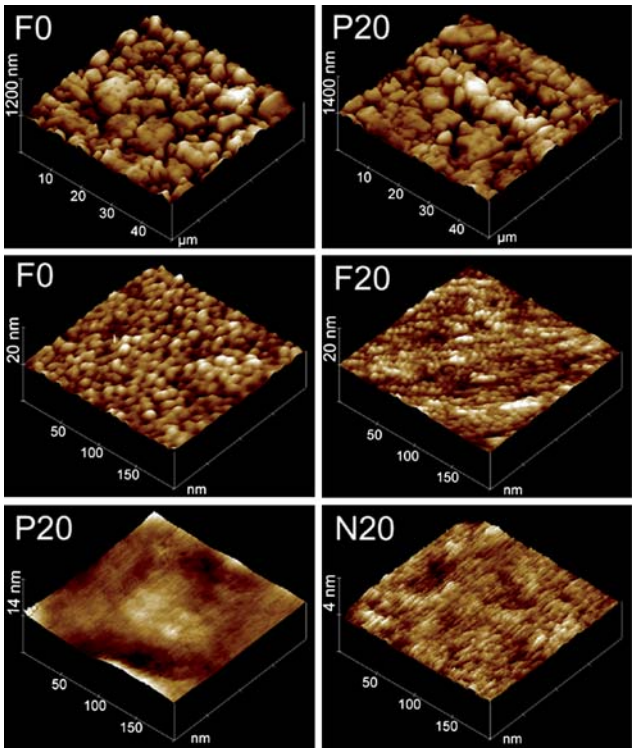

Fig. 4 AFM images of the MBG coatings (F0, P20 and N20).

coatings showed arranged islands and pits with diameters of about 6–10 nm (Fig. 4), which was in agreement with the results shown in Fig. 1–3. However, the depth of the pits was only about 2 nm, as determined by AFM. By combining N_2 adsorption/desorption and TEM results, it can be inferred that the pits with diameters of about 6–10 nm of F0 and F20 in the AFM images should correspond to the mesopores as shown in Fig. 1–3. On the other hand, P123 generally showed a 2D mesoporous texture with pore channels aligned parallel to the substrate surface (Fig. 1–3).[20–26] In the 200-nm area image, the P20 coating showed a smooth surface without any obvious pits or islands, which was very similar to N20 (Fig. 4). The TEM image of P20 revealed an ordered 2D arrangement of one-dimensional channels with a diameter of about 4 nm (Fig. 2 and 3). This channel structure was presented under the coating surface and explained why no nano-texture like that shown in F0 and F20 was observed by AFM on the surface of P20. Moreover, the various chemical compositions of the coatings were easily achieved by changing the composition of the sol solutions. With the addition of calcium and phosphorus, the crystallinity of the MBG coating increased and thus the BET surface area decreased: the BET surface area of F0, F20, P20 and F30 were 364, 145, 185 and 170 $m^2\ g^{-1}$, respectively (Fig. 2 and Table S2, ESI†).

The obtained MBG coatings were found to homogeneously spread on the stainless steel plate (Fig. 4). In the 50-μm-area image, all the coatings showed rough surfaces, which were inherited from the stainless steel plate (representative images of F0 and P20 are shown in Fig. 4). The thickness of the MBG coating was about 5–10 μm as shown by the cross section of the MBG coating (Fig. S1, ESI†). The thin-film X-ray diffraction (TF-XRD) patterns of the MBG coatings showed a broad diffraction peak at approximately 20–30° and indicated that the main phase of the MBG coatings was silicate (Fig. 1).

The proteins in fetal bovine serum (FBS) containing cell culture medium were well adsorbed on the surface of the MBG coating when the MBG-coated stainless steel plate was soaked in cell culture medium. Through the adsorbed protein layers, the attachment, spreading, cytoskeletal organization, proliferation and differentiation of osteoblastic MC3T3-E1 cells can be affected by the mesoporous texture and chemical composition of the MBG coatings. The amount of proteins adsorbed to F20 was higher than those of the proteins adsorbed to F0, N0, P20, N20, F30 and N30 (Fig. 5). The presence of mesopores offered the possibility of adsorbing or entrapping large biomolecules within their pores as well as on the external surface area.[27] For instance, 6–10 layers of cytochrome c could form on the external surface of mesoporous materials.[27] Moreover, the pore size and texture were important factors in affecting the protein adsorption behaviour of mesoporous materials. The MBG coatings with 3D mesoporous texture facilitate faster transport and adsorption of bioactive agents (such as proteins and nutrients) than the 2D textures, because of their different diffusion mechanisms and accessibilities.[9,11] In addition, the chemical composition of the MBG coating is another important factor that affects the protein adsorption. The MBG coating with higher calcium contents tend to create more unstable glasses whereas lower calcium contents result in bioinert behaviour.[7] When the calcium content in the glass decreased, the network becomes more compact and closed due to an increase in bridging bonds (Si–O–Si) that hold the network together. In contrast, when the calcium level was increased, the distribution of the network grows due to an increase in nonbridging oxygen between Si and Ca. Therefore, an increase in the calcium content of the glasses results in a more bioactive behaviour by virtue of easier diffusion of ions through the glass.[2]

The protein adsorption capabilities and ion concentrations in the cell culture medium, which originated from the mesoporous texture and chemical composition of the MBG coatings, were responsible for the differences in the osteoblastic MC3T3-E1 cell attachment, proliferation and differentiation on the MBG coatings. The number of osteoblastic MC3T3-E1 cells attached to the MBG coating at the early stage (1 h) showed the same tendency as the amount of protein adsorbed (Fig. 5 and 6(A)). With longer incubation time, an increase in cell number was

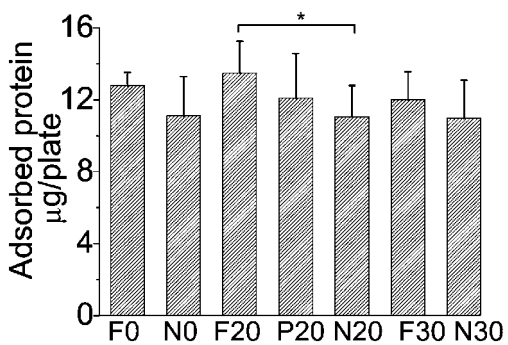

Fig. 5 Protein adsorption on the MBG coatings after 2 h immersion in culture medium.

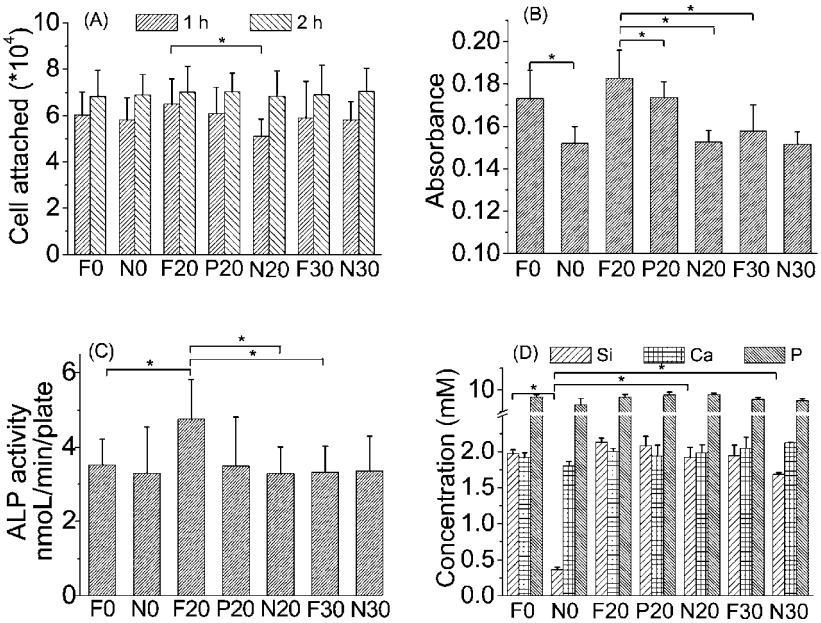

Fig. 6 Osteoblast MC3T3-E1 cell culture. Osteoblast MC3T3-E1 cell attachment onto the MBG coatings after 1 and 2 h immersion in culture medium (A); osteoblast MC3T3-E1 cell proliferation on the MBG coatings after 7 days of culture (B); ALP activity of osteoblast MC3T3-E1 cells on the MBG coatings after 7 days of culture (C); silicon, calcium and phosphorus concentrations in the osteoblast MC3T3-E1 cell culture medium after 3 days of culture (D).

observed for all the specimens. Cell attachment and spreading involve the following steps:[12] (1) adsorption of proteins on the coating surface; (2) contact and attachment of cells onto the protein layer; (3) centrifugal growth of filopodia; (4) cytoplasma spreading; and (5) cell flattening. Proteins, including collagen, fibronectin, vitronectin and laminin, exist in FBS in great varieties and amounts. The adsorption of proteins plays a key role in the subsequent osteoblastic MC3T3-E1 cell attachment and eventual cell morphology. Proteins are well adsorbed on the MBG coating surface once the protein comes into contact with the coating because the MBG coatings are intrinsically highly surface-active. Through this adsorbed protein layer, the cells sense and attach to foreign surfaces.[12] The more protein is adsorbed, the more anchorages would be provided for osteoblastic MC3T3-E1 cell attachment.[12] Indeed, the different mesoporous textures and chemical compositions of the MBG coatings affected the protein adsorption and the subsequent initial cell attachment. The initial cell attachment and subsequent spreading are crucial prerequisites in the determination of the long-term viability of cells on the implant surface, involving cell proliferation, differentiation, mineralization and successful osteointegration of anchorage-dependent cells (such as osteoblastic MC3T3-E1 cells).[8,10] The osteoblastic MC3T3-E1 cell proliferation and differentiation on F20 was significantly higher than those on F0, N0, P20, N20, F30 and N30 (Fig. 6(B) and (C)). Besides, the silicate dissolved in the cell culture medium is key factor that control the proliferation, protein synthesis and ALP activity of osteoblasts, and also the formation and development of bone tissue.[28–32] Previous studies showed that less than 2.50 mM silicon in the cell culture medium enhances proliferation, protein synthesis and ALP activity of osteoblasts, and also enhances the formation and development of bone tissue.[28–32] However, high dose silicate may result in toxicity.[33] The MBG coatings released silicon to a level of about 0.4–2.1 mM in the cell culture medium, which accounts for the enhanced osteoblast

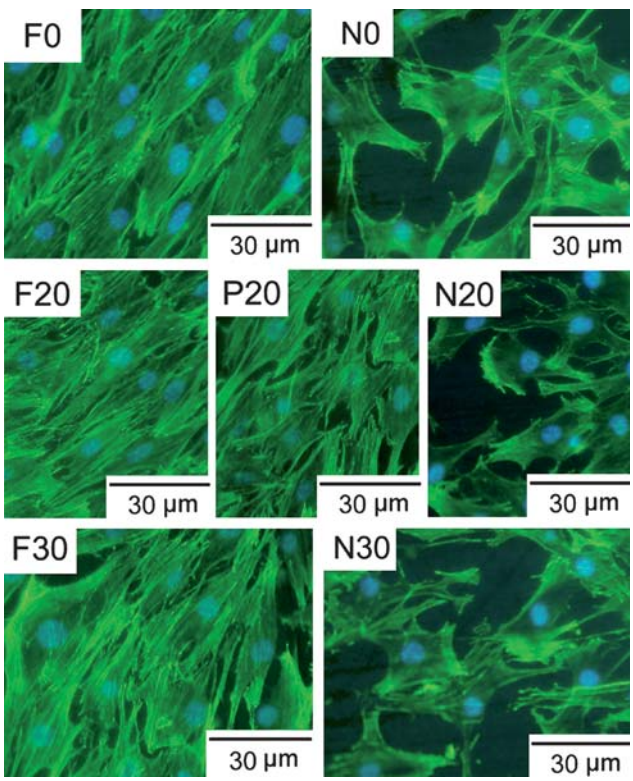

Fig. 7 Fluorescent micrographs of F-actin labeled cytoskeleton of osteoblast MC3T3-E1 cells after 7 days of culture on the MBG coatings.

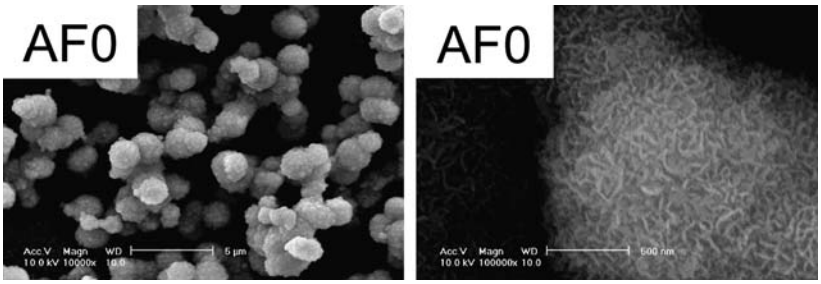

Fig. 8 SEM micrograph of the AsMg-immobilized-MBG coatings.

MC3T3-E1 cell proliferation and ALP activity. The use of triblock copolymers, calcium and phosphorus greatly increased the amount of silicate dissolved into the cell culture medium (1.7–2.1 mM silicon for F0, F20, P20, N20, F30 and N30, 0.4 mM silicon for N0, Fig. 6(D)), which accounted for the enhanced osteoblastic MC3T3-E1 cell proliferation and ALP activity. Note that the osteoblastic MC3T3-E1 cells were cultured on the MBG coatings directly in the culture medium. This fact suggested that both the mesoporous texture and ion release of the MBG coatings affected osteoblastic MC3T3-E1 cell proliferation and differentiation *in vitro*.

The introduction of mesoporous texture in the MBG coatings (Fig. 1–4) resulted in an increase in F-actin alignment (Fig. 7). The cells attached to N0, N20 and N30 exhibited F-actin stress fibers, which emanate from the nucleus toward the structural points of contact between the cell and the substrate in a radial fashion (Fig. 7). Interestingly, on mesoporous-texture-modified substrates (F0, F20, P20 and F30), the F-actin fibers span almost the entire length of the cell (Fig. 7). Moreover, there was a tendency in cell shape: a spindle like elongated shape was mostly observed on F0, F20, F30 and P20 coatings, while on the N0, N20 and N30 coatings, the general shape was polygonal. In addition, the minor/major axis ratio was lower on the F0, F20, F30 and P20 surfaces than on the N0, N20 and N30 surfaces. The mesoporous textures in F0, F20, F30 and P20 (Fig. 1–4) should account for the increase in F-actin alignment, compared with that in the case of N0, N20 and N30, regardless of the similarity in micrometre-scale roughness inherited from the stainless steel plate. Although P20 showed no mesoporous textures in its surface AFM image (Fig. 4), the quick exposure of the interior mesoporous textures confirmed by N_2 adsorption/desorption, TEM and XRD (Fig. 1–3) was expected owing to the partial dissolution of the coatings when immersed in the cell culture medium. It is reported that nano sized features such as islands,

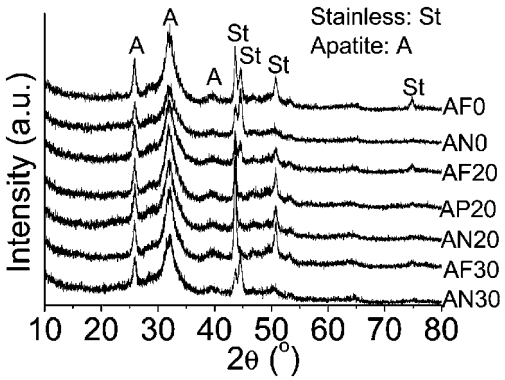

Fig. 9 XRD patterns of the AsMg-immobilized-MBG coatings.

grooves and pits in a size range of 5–500 nm affected the cytoskeletal organization[14,15,34] owing to the protein adsorption and changes in cell membrane tension.[35]

By using an AsMg-containing supersaturated calcium phosphate solution, AsMg was successfully loaded on the MBG coatings. A continuous and homogeneous layer with fine flakes of about 5–10 nm thickness and 50–100 nm length was formed on the AsMg-MBG coatings (Fig. 8 and S2, ESI†). Some fine flakes gathered and formed into round particles with diameter of 1–2 μm. The AsMg-MBG coatings consisted of low-crystalline apatite (ICDD No. 09-432, Fig. 9). AF20 showed the maximum AsMg and calcium loading (Fig. 10(A) and (B)). The AsMg, calcium and phosphorus immobilization ability are highly related to the mesoporous texture and chemical composition of the MBG coatings. Increasing the porosity and specific surface area is especially important to accelerate the kinetic of immobilizing AsMg, calcium and phosphorus on the MBGs. The AsMg loaded in this study was not denatured and showed high activity

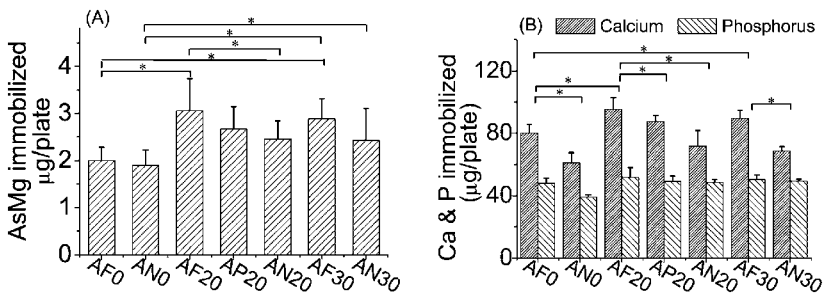

Fig. 10 Amounts of AsMg (A), calcium and phosphorus (B) loaded on the AsMg-MBG coatings.

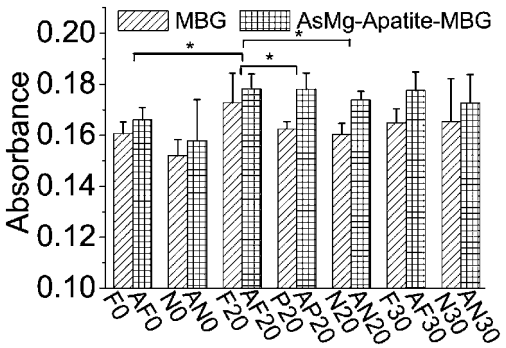

Fig. 11 Fibroblast NIH3T3 cell proliferation on the MBG and AsMg-MBG coatings after 72 h of culture.

enhancing the fibroblastic NIH3T3 cell proliferation *in vitro* (Fig. 11). Ascorbic acid has been shown to stimulate collagen synthesis in cultured dermal fibroblasts through stimulation of the expression of collagen genes for the α1(I), α2(I), α1(III) and α1(IV) chains.[36,37] Moreover, AF20 showed highest fibroblastic NIH3T3 cell proliferation. The fibroblastic NIH3T3 cells on the MBG coatings after 72 h of culture in the serum-free cell culture medium remained a round shape without obvious pseudopods. By contrast, the fibroblastic NIH3T3 cells on the AsMg-MBG coatings after 72 h of culture in the serum-free cell culture medium spread well and showed polygonal shape with obvious pseudopods (Fig. 12 and S4, ESI†).

Conclusions

Cooperative organic–inorganic self-assembly reactions of triblock copolymers and inorganic precursors resulted in MBG coatings on stainless steel plates, by spin-coating of a sol solution. The use of different triblock copolymers permitted the channel texture to be modified in the mesoscopic regime. With the addition of calcium and phosphorus, the crystallinity of the MBG coatings increased and thus the BET surface area and the pore volume decreased. The mesoporous texture and release of silicate should be responsible for the protein adsorption, osteoblastic MC3T3-E1 cell attachment, proliferation, differentiation, cytoskeletal organization and AsMg immobilization. Moreover, the AsMg loaded was not denatured and showed high activity enhancing the fibroblastic NIH3T3 cell proliferation *in vitro*. The possibility of designing the texture of BG at a nanoscale level, through the use of triblock copolymers as mesoporous directing agents, may be a valid and promising route to prepare the bioactive coatings.

Acknowledgements

We thank the technical assistance in TEM imaging of Dr Noriko Yoshizawa, Energy Technology Research Institute, National Institute of Advanced Industrial Science and Technology (AIST). This study was supported in part by the Industrial Technology Research Grant Program in 2005 from the New Energy and Industrial Technology Development Organization (NEDO) of Japan and by a Grant-in-Aid for Scientific Research (JSPS postdoctoral fellowship) No. 19-07608 from the Japan Society for the Promotion of Science (JSPS).

References

1 M. H. Fathi and A. D. Mohammadi, *Mater. Sci. Eng., A*, 2008, **474**, 128–133.
2 J. M. Gomez-Vega, A. Hozumi, E. Saiz, A. P. Tomsia, H. Sugimura and O. Takai, *J. Biomed. Mater. Res.*, 2001, **56**, 382–389.
3 S. H. Maxian, J. P. Zawadsky and M. G. Dunn, *J. Biomed. Mater. Res.*, 1993, **27**, 717–728.
4 C. P. Klein, J. G. Wolke, J. M. de Blieck-Hogervorst and K. de Groot, *J. Biomed. Mater. Res.*, 1994, **28**, 961–967.
5 A. M. Lipski, C. J. Pino, F. R. Haselton, I. W. Chen and V. P. Shastri, *Biomaterials*, 2008, **29**, 3836–3846.
6 M. A. Schwartz and M. H. Ginsberg, *Nat. Cell Biol.*, 2002, **4**, E65–68.
7 L. L. Hench, *J. Am. Ceram. Soc.*, 1991, **74**, 1487–1510.
8 D. S. Kommireddy, S. M. Sriram, Y. M. Lvov and D. K. Mills, *Biomaterials*, 2006, **27**, 4296–4303.
9 A. López-Noriega, D. Arcos, I. Izquierdo-Barba, Y. Sakamoto, O. Terasaki and M. Vallet-Regí, *Chem. Mater.*, 2006, **18**, 3137–3144.
10 S. N. Nayab, F. H. Jones and I. Olsen, *Biomaterials*, 2005, **26**, 4717–4727.
11 H.-s. Yun, S.-e. Kim and Y.-t. Hyun, *Solid State Sci.*, 2007, 1–10.
12 Y. Wang, S. Zhang, X. Zeng, L. L. Ma, K. A. Khor and M. Qian, *J. Biomed. Mater. Res., Part A*, 2008, **84a**, 769–776.
13 D. J. Hulmes, *J. Struct. Biol.*, 2002, **137**, 2–10.
14 E. Eisenbarth, D. Velten, M. Muller, R. Thull and J. Breme, *J. Biomed. Mater. Res., Part A*, 2006, **79a**, 166–175.
15 M. J. Dalby, S. J. Yarwood, M. O. Riehle, H. J. Johnstone, S. Affrossman and A. S. Curtis, *Exp. Cell Res.*, 2002, **276**, 1–9.
16 C. J. Bettinger, R. Langer and J. T. Borenstein, *Angew. Chem., Int. Ed.*, 2009, **48**, 5406–5415.
17 M. J. Dalby, M. O. Riehle, H. J. Johnstone, S. Affrossman and A. S. Curtis, *Tissue Eng.*, 2002, **8**, 1099–1108.
18 E. Soheili Majd, M. Goldberg and L. Stanislawski, *Biomaterials*, 2003, **24**, 3–9.
19 M. C. Ronzière, S. Roche, J. Gouttenoire, O. Demarteau, D. Herbage and A. M. Freyria, *Biomaterials*, 2003, **24**, 851–861.
20 D. Zhao, P. Yang, N. Melosh, J. Feng, B. F. Chmelka and G. D. Stucky, *Adv. Mater.*, 1998, **10**, 1380–1385.
21 J. M. Gomez-Vega, A. Hozumi, H. Sugimura and O. Takai, *Adv. Mater.*, 2001, **13**, 822–825.

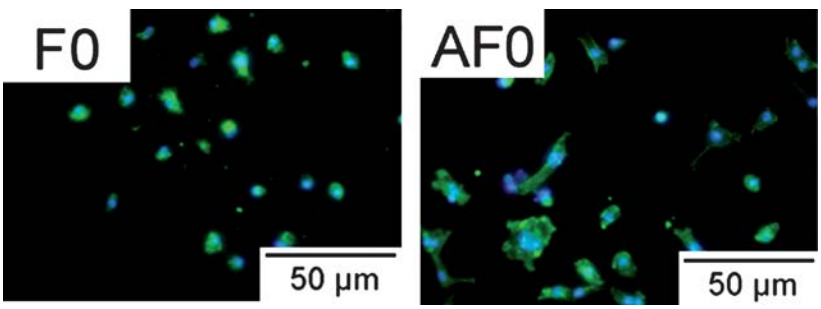

Fig. 12 Fluorescent micrographs of F-actin labeled cytoskeleton of fibroblast NIH3T3 cells after 72 h of culture on the MBG (left) and AsMg-immobilized-MBG coatings (right).

22 J. M. Gomez-Vega, M. Iyoshi, K. Y. Kim, A. Hozumi, H. Sugimura and O. Takai, *Thin Solid Films*, 2001, **398–399**, 615–620.
23 X. Li, X. P. Wang, H. R. Chen, P. Jiang, X. P. Dong and J. L. Shi, *Chem. Mater.*, 2007, **19**, 4322–4326.
24 X. Li, X. P. Wang, D. N. He and J. L. Shi, *J. Mater. Chem.*, 2008, **18**, 4103–4109.
25 X. X. Yan, X. H. Huang, C. Z. Yu, H. X. Deng, Y. Wang, Z. D. Zhang, S. Z. Qiaoc, G. Q. Lu and D. Y. Zhao, *Biomaterials*, 2006, **27**, 3396–3403.
26 X. X. Yan, C. Z. Yu, X. F. Zhou, J. W. Tang and D. Y. Zhao, *Angew. Chem., Int. Ed.*, 2004, **43**, 5980–5984.
27 S. Hudson, J. Cooney and E. Magner, *Angew. Chem., Int. Ed.*, 2008, **47**, 8582–15.
28 E. M. Carlisle, *Science (New York, N.Y)*, 1970, **167**, 279–280.
29 D. M. Reffitt, N. Ogston, R. Jugdaohsingh, H. F. Cheung, B. A. Evans, R. P. Thompson, J. J. Powell and G. N. Hampson, *Bone*, 2003, **32**, 127–135.
30 A. M. Pietak, J. W. Reid, M. J. Stott and M. Sayer, *Biomaterials*, 2007, **28**, 4023–4032.
31 I. D. Xynos, A. J. Edgar, L. D. Buttery, L. L. Hench and J. M. Polak, *J. Biomed. Mater. Res.*, 2001, **55**, 151–157.
32 P. Valerio, M. M. Pereira, A. M. Goes and M. F. Leite, *Biomaterials*, 2004, **25**, 2941–2948.
33 S. R. Blumen, K. Cheng, M. E. Ramos-Nino, D. J. Taatjes, D. J. Weiss, C. C. Landry and B. T. Mossman, *Am. J. Respir. Cell Mol. Biol.*, 2006, **36**, 333–342.
34 M. J. Dalby, S. J. Yarwood, H. J. Johnstone, S. Affrossman and M. O. Riehle, *IEEE Trans. NanoBiosci.*, 2002, **1**, 12–17.
35 T. J. Webster, L. S. Schadler, R. W. Siegel and R. Bizios, *Tissue Eng.*, 2001, **7**, 291–301.
36 R. I. Hata and H. Senoo, *J. Cell. Physiol.*, 1989, **138**, 8–16.
37 S. Murad, D. Grove, K. A. Lindberg, G. Reynolds, A. Sivarajah and S. R. Pinnell, *Proc. Natl. Acad. Sci. U. S. A.*, 1981, **78**, 2879–2882.